Available online at www.sciencedirect.com
ScienceDirect
Polymer 48 (2007) 5671–5680
polymer
www.elsevier.com/locate/polymer

Epoxy/polyhedral oligomeric silsesquioxane (POSS) hybrid networks cured with an anhydride: Cure kinetics and thermal properties

Jun Kai Herman Teo [a], Kiat Choon Teo [b], Binghua Pan [b], Yang Xiao [a,c], Xuehong Lu [a,*]

[a] School of Materials Science and Engineering, Nanyang Technological University, 50 Nanyang Avenue, Singapore 639798, Singapore
[b] Delphi Automotive Systems Singapore Pte. Ltd., 501 Ang Mo Kio Industrial Park I, Singapore 569621, Singapore
[c] Institute of Materials Science and Engineering, 3 Research Link, Singapore 117602, Singapore

Received 26 February 2007; received in revised form 10 July 2007; accepted 25 July 2007
Available online 1 August 2007

Abstract

A new class of organic–inorganic hybrid networks was prepared *via* copolymerization of octakis(dimethylsiloxybutyl epoxide)octasilsesquioxane (OB), *N*,*N*,*N*′,*N*′-tetraglycidyl-4,4′-diaminodiphenyl methane (TGDDM) and hexahydrophthalic anhydride (HHPA). Kinetic studies show that even with 1H-imidazole as the catalyst, the rate for the curing of OB/HHPA is still significantly higher than that for TGDDM/HHPA in the temperature range studied. Two-stage reactions were thus carried out to allow OB to react with HHPA first (Stage I). The glass transition temperature (T_g) of the networks was found to be strongly dependent on Stage I reaction since too short a reaction time caused poor bonding of OB to the networks while too long a reaction time led to the formation of OB oligomers that de-homogenized the networks. With 5 mol.% OB, the hybrid prepared *via* the optimized two-stage reaction displayed a large jump of ~20 °C in T_g, which was accompanied by slight improvements in thermal degradation temperature and storage modulus, as compared to TGDDM/HHPA.

Keywords: Polyhedral oligomeric silsesquioxane (POSS); Networks; Cure kinetics

1. Introduction

Polyhedral oligomeric silsesquioxanes (POSSs) have received considerable attention recently as they possess a synergistic combination of constituent properties of organic and inorganic materials. Incorporation of functional POSS into thermosetting polymers, such as epoxies, allows for the modifications of the composition and network structure of the polymers simultaneously so that these material systems often exhibit dramatic improvements in performance. This makes them potentially useful for many engineering applications, one of which is in the field of electronic packaging. The characteristics of the epoxy/POSS networks such as high glass transition temperature (T_g), low density, excellent oxidation resistance and high mechanical strength will be a boon in improving the global properties of the electronic packaging materials [1,2].

A number of research groups have prepared hybrid networks from various types of epoxy-functionalized POSS with diamines as the curing agents [3–17]. An alternative approach was to use amine-functionalized POSS as hardeners for curing epoxies [18,19]. Both approaches yielded hybrid networks with improved T_gs, thermal degradation temperatures (T_ds) and thermo-mechanical properties. More recently, Laine et al. developed a novel class of epoxy/POSS networks with very low coefficients of thermal expansion (CTE) using octaaminophenylsilsesquioxane as the curing agent [19]. The combined use of dicyandiamide and a phosphorus-containing compound as curing agents for epoxy-functionalized POSS to improve homogeneity as well as flame retardant properties of the resultant hybrids has also been reported [20,21]. To date, most studies on the preparation of the epoxy/POSS

* Corresponding author. Tel.: +65 6790 4585; fax: +65 6790 9081.
E-mail address: asxhlu@ntu.edu.sg (X. Lu).

0032-3861/$ - see front matter © 2007 Elsevier Ltd. All rights reserved.
doi:10.1016/j.polymer.2007.07.059

networks have, however, mainly revolved around the use of amine-based curing agents. There was only one publication so far detailing the investigation of an epoxy/POSS system with carboxylic acid anhydride as the curing agent, which reported some improvements in properties at rubbery state [22]. Being high-temperature curing agents, anhydrides do not react with epoxies at room temperature. On the other hand, with the aid of suitable catalysts, they are able to cure epoxies quickly at elevated temperatures, and the cure profiles can be manipulated conveniently by varying the type and the amount of the catalyst [23,24]. This is highly desirable for some electronic packaging materials, such as no-flow underfills used in flip-chip technology, for which premature curing must be prevented to ensure excellent flow properties whereas the cure must also proceed rapidly in a narrow processing temperature window determined by solder bump reflow temperatures. In addition, epoxy/anhydride systems may also provide better electrical insulation properties [25].

In this work, we report on the preparation of epoxy-based hybrid networks containing octakis(dimethylsiloxybutyl epoxide)octasilsesquioxane (OB) with hexahydrophthalic anhydride (HHPA) as the curing agent and 1H-imidazole as the catalyst. *N*,*N*,*N*′,*N*′-Tetraglycidyl-4,4′-diaminodiphenyl methane (TGDDM), a widely used epoxy compound in electronic packaging materials, was used as a co-monomer. Cure kinetics of the OB/HHPA and TGDDM/HHPA systems were studied. The progress of the cure reactions was monitored to elucidate the influence of the reactions on the thermal and thermomechanical properties of the resultant hybrid materials. The morphology of the nanocomposites was also investigated to correlate the homogeneity of the POSS dispersion to the resultant thermal properties of the hybrid materials.

2. Experimental

2.1. Materials

Octakis(dimethylsiloxy)octasilsesquioxane ($Q_8M_8^H$) was purchased from Hybrid Plastics Co. 1,2-Epoxy-5-hexene, anhydrous toluene and TGDDM (epoxide equivalent weight = 110–115 g/equiv.) were obtained from Aldrich Chemical Co. Platinum divinyltetramethyldisiloxane complex was purchased from Aldrich and diluted to a 2 mM solution in anhydrous toluene. HHPA (≥95%) and 1H-imidazole was obtained from Fluka. OB was synthesized in our laboratory according to the method reported by He's group [8]. The structure and purity of OB prepared were verified by NMR, Fourier transform infrared (FTIR) spectroscopy, matrix-assisted laser desorption/ionization time-of-flight mass spectroscopy (MALDI-TOF-MS) and elemental analysis. ^{1}H NMR ($CDCl_3$) (δ, ppm): 0.14 [Si(CH_3)$_2$CH$_2$], 0.63 (SiMe$_2$$CH_2CH_2$), 1.43–1.52 (SiMe$_2CH_2$$CH_2$$CH_2$$CH_2$ epoxy), 2.44 (CH_2 epoxy), 2.73–2.89 (CH epoxy). ^{13}C NMR ($CDCl_3$) (δ, ppm): −0.01 [Si(CH_3)$_2$CH$_2$], 17.8 (SiMe$_2$$CH_2CH_2$), 23.1 (SiMe$_2CH_2$$CH_2CH_2$), 29.8 (SiMe$_2CH_2CH_2$$CH_2CH_2$), 32.5 (SiMe$_2CH_2CH_2CH_2$$CH_2$ epoxy), 47.3 (CH epoxy), 52.4 (CH_2 epoxy). ^{29}Si NMR ($CDCl_3$) (δ, ppm): −100.4 (*Si*–O–*Si*), 20.9 (O*Si*Me$_2$). FTIR (KBr, cm^{-1}): 2946 (υ-CH), 1090, 770 (υ-Si–O–Si), 916 (δ-C–O), 846 (υ-C–O). MALDI-TOF-MS: calcd. molecular weight = 1803.1. Found 1801.7. $C_{64}H_{136}O_{28}Si_{16}$: calcd. C, 42.67; H, 7.55. Found: C, 42.54; H, 7.29.

2.2. Preparation of hybrid networks

The chemical structures of the compounds used in the preparation of the hybrid networks are shown in Scheme 1.

Stoichiometric ratio of epoxide/anhydride = 2 was used for all samples, including the ones for cure kinetics study. The concentration of OB in the resins was defined according to the relationship below,

$$\text{OB conc. (mol.\%)} = \frac{\text{Number of moles of OB}}{\text{Number of moles of (OB + TGDDM)}} \times 100$$

The catalyst concentration was defined as the molar ratio of 1H-imidazole/HHPA. The OB/TGDDM/HHPA resins were prepared by first pre-mixing OB and HHPA with the catalyst at 110 °C for a certain time period (Stage I) and then quenching the precursor in ice. TGDDM was then mixed with the precursor homogeneously at room temperature. The mixture was degassed under vacuum at ~40 °C. It was then poured into an aluminium mould coated with a mould-releasing agent, cured in a Memmert air-circulating convection oven at 140 °C and then post-cured in an inert-gas-purged oven at 200 °C (Stage II). TGDDM/HHPA and OB/HHPA resins were prepared accordingly but omitting Stage I. The compositions of the resins and the conditions for the cure are summarized in Table 1.

2.3. Cure kinetics

Cure kinetics was studied by differential scanning calorimetry (DSC) using a TA Instruments DSC 2010 in nitrogen

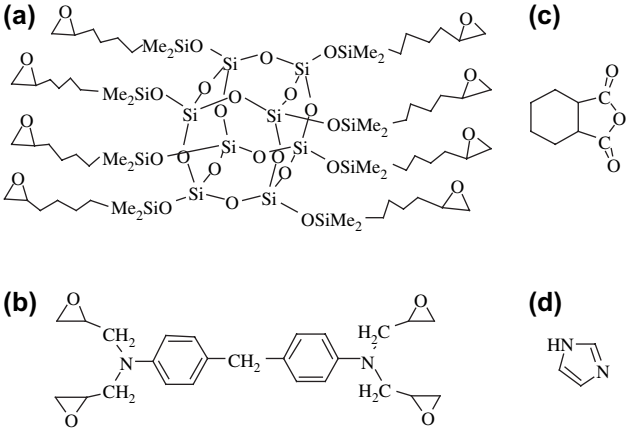

Scheme 1. Chemical structures of (a) OB; (b) TGDDM; (c) HHPA; (d) 1H-imidazole.

Table 1
Compositions and curing conditions for the preparation of the hybrid networks

Sample	OB conc. (mol.%)	OB conc. (wt.%)	Catalyst/HHPA molar ratio	Reaction time		
				Stage I at 110 °C (min)	Stage II (h)	
					First cure at 140 °C	Post-cure at 180 °C
TGDDM/HHPA	0	0.0	0.009	0	1	4, 24
5 mol.% OB-0	5	11.0	0.009	0	1	4, 24, 72
5 mol.% OB-10	5	11.0	0.009	10	1	24
5 mol.% OB-15	5	11.0	0.009	15	1	24
5 mol.% OB-20	5	11.0	0.009	20	1	24
5 mol.% OB-10-H	5	11.0	0.027	10	1	24
10 mol.% OB-10	10	20.0	0.009	10	1	24
OB/HHPA	100	74.5	0.009	0	1	24
OB/HHPA-H	100	74.5	0.09	0	1	24

atmosphere. TGDDM/HHPA and OB/HHPA mixtures with the catalyst concentration of 0.09 mol.% were prepared and ~5 mg each was sealed in a hermetic pan. The rate of reaction of the mixtures was monitored at an isothermal temperature of 140 °C until no further heat flow can be detected. The mixtures were also heated at four different heating rates (5, 10, 15 and 20 °C/min) from 25 to 300 °C.

2.4. Monitoring of Stage I reaction

2.4.1. DSC

To simulate Stage I reaction, 5 mol.% OB and 0.009 mol.% 1H-imidazole were mixed with HHPA and sealed in hermetic pans. Isothermal heating scans were recorded at 110 °C for 60 min using a TA Instruments DSC 2010 in nitrogen atmosphere.

2.4.2. FTIR

The samples collected at different pre-mixing time were cast on circular BaF_2 plates, and the FTIR spectra were obtained using a Perkin–Elmer Instruments Spectrum GX FTIR spectrometer at room temperature from 700 to 4000 cm^{-1}. A total of 20 scans were recorded at a resolution of 4 cm^{-1} for averaging each spectrum.

2.4.3. SEC

The samples collected at different pre-mixing times were dissolved in chloroform, and the SEC measurements were carried out using an Agilent Technologies 1100 Series GPC analysis system calibrated with polystyrene standards with chloroform as the eluant at a flow rate of 1.0 ml/min.

2.5. Characterization

2.5.1. Scanning electron microscopy (SEM)

Morphological studies were carried out using a JEOL JSM 6340F field emission scanning electron microscope. The samples were fractured cryogenically using liquid nitrogen and the fractured surfaces were applied to the SEM measurements.

2.5.2. DSC

T_gs were determined by a TA Instruments DSC 2010 under nitrogen purge from 30 to 300 °C at a heating rate of 10 °C/min. The inflexion point of the transition region was taken to be the T_gs of the samples.

2.5.3. Thermogravimetric analysis (TGA)

The thermal stability of the cured resins was investigated by a TA Instruments High Resolution TGA 2950 thermogravimetric analyzer over a temperature range of 80–700 °C under nitrogen (20 ml/min) at a heating rate of 20 °C/min. The temperature at 5% weight loss was taken as the thermal degradation temperature ($T_d^{5\%}$).

2.5.4. Dynamic mechanical analysis (DMA)

Storage moduli of the cured samples were recorded with a dynamic mechanical analyzer DMA Q800 from TA Instruments. The samples were polished to ~17.5 × 13.0 × 3.0 mm before being mounted on a single cantilever clamp and measured at a frequency of 1.0 Hz and a heating rate of 3 °C/min from 25 to 250 °C.

2.5.5. Thermo-mechanical analysis (TMA)

CTE measurements were conducted using a TA Instruments TMA 2940 thermo-mechanical analyzer at a heating rate of 3 °C/min from room ambient to 250 °C in a nitrogen atmosphere.

3. Results and discussion

3.1. Effect of catalyst concentration

The cure profiles of OB/HHPA and TGDDM/HHPA are depicted in Fig. 1a and b, respectively. Without any catalyst, the cure peak temperature of OB/HHPA reached 400 °C (curve I in Fig. 1a). Too high a cure temperature would result in excessive evaporation and decomposition of the reaction mixtures, thus a catalyst has to be added to help to bring the cure temperature to feasible values. With 1H-imidazole as the catalyst, the cure peaks were shifted to much lower temperatures. The

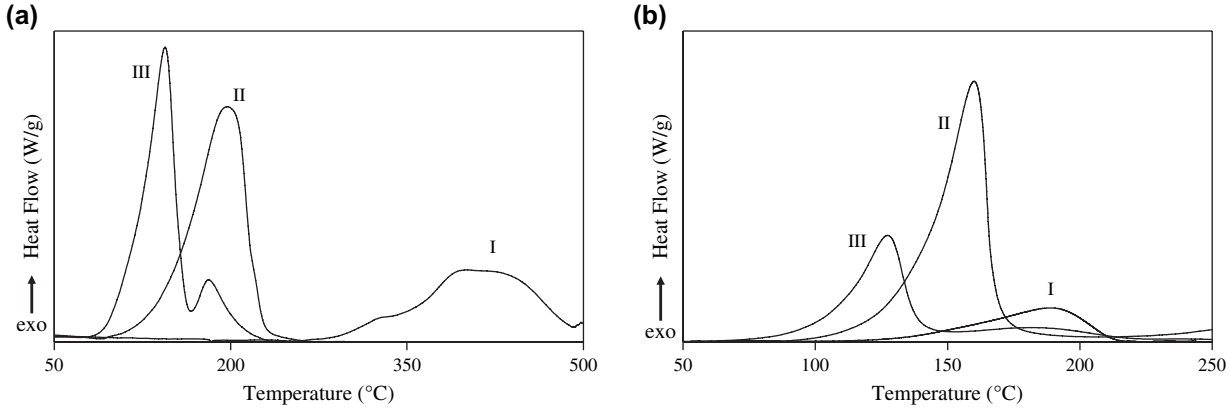

Fig. 1. DSC thermograms of (a) OB/HHPA and (b) TGDDM/HHPA with the catalyst/HHPA molar ratio of 0 (I), 0.009 (II) and 0.09 (III).

higher the catalyst concentration, the larger will be the shift (Fig. 1a).

The reaction mechanism of the anhydride with the epoxy is depicted in Scheme 2. It shows that the increased reactivity of the systems is brought by the interactions of the amine site in 1H-imidazole with the anhydride and epoxide groups, which produce adducts containing highly reactive alkoxide ions to initiate the rapid anionic copolymerization, i.e. esterification, between epoxies and HHPA [26,27]. It is worth noting that some alkoxide ions produced in step 3 in Scheme 2 may not be able to react with HHPA due to the steric hindrance posed by the OB attached [3,14]. A relatively high epoxy/anhydride ratio was thus used in this study. The excess amount of epoxy may cause homopolymerization, i.e. etherification between the epoxide groups, to some extent.

TGDDM was chosen as a co-monomer in this study because it has four short arms with reactive sites so that it can potentially give high cross-linking density and hence the desirable properties. The addition of TGDDM into the reaction mixtures brings in, however, a reaction that is in competition with the one between OB and HHPA. Fig. 1b shows that the cure peak for TGDDM/HHPA was located at a much lower temperature, as compared to that of OB/HHPA, when no catalyst was used. This is due to the fact that there are internal catalytic sites (tertiary amine) in TGDDM to catalyze the anhydride ring opening [28]. With the catalyst, the cure peak temperatures of the TGDDM/HHPA system also reduced, but to a less extent as compared to the shifts for the OB/HHPA system. Thus, as the catalyst concentration increased, the cure peaks for OB/HHPA and TGDDM/HHPA became closer to each other.

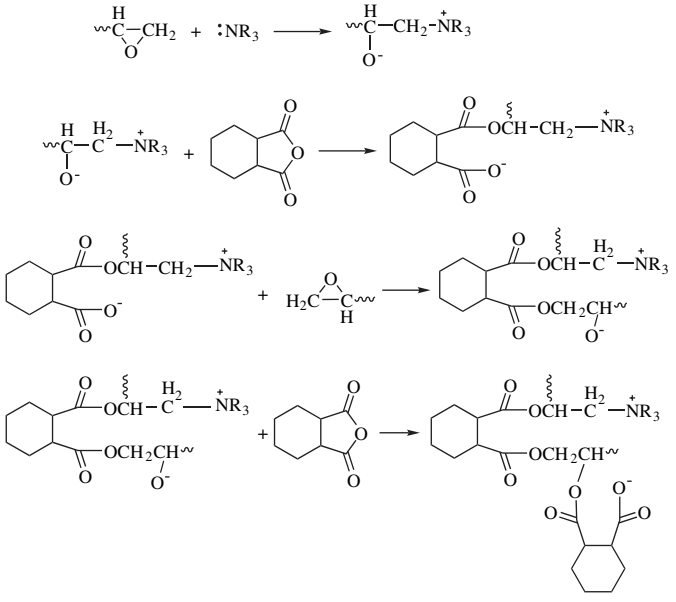

Scheme 2. Schematic cure mechanism of catalyzed epoxy/anhydride system.

3.2. Cure kinetics

To compare the reaction rates of OB/HHPA and TGDDM/HHPA systems in the presence of the catalyst, isothermal DSC experiments were carried out at 140 °C for OB/HHPA and TGDDM/HHPA with the same catalyst concentration. The results are presented in Fig. 2. Obviously, TGDDM reacts with HHPA much faster than OB at this particular temperature. Isothermal DSC experiments conducted at 110 and 200 °C showed similar trends. However, they could not yield a proper conversion versus time curve as the reaction between OB and HHPA at 110 °C was too slow while the one between TGDDM and HHPA at 200 °C was too fast to be captured properly.

To further compare the reactivities of OB and TGDDM towards HHPA in the presence of the catalyst, a dynamic kinetic analysis was performed using two established non-isothermal kinetic models: the Kissinger and Flynn–Wall–Ozawa models [29–31]. Both models do not require prior knowledge of the reaction mechanism.

According to Kissinger model, the activation energy can be obtained from the equation below [32],

$$\frac{\mathrm{d}\left[\ln\left(q/T_{\mathrm{peak}}^2\right)\right]}{\mathrm{d}\left(1/T_{\mathrm{peak}}\right)} = -\frac{E_{\mathrm{a}}}{R} \tag{1}$$

where T_{peak} is the peak exotherm temperature, q the constant heating rate, E_{a} the activation energy of the reaction, and R

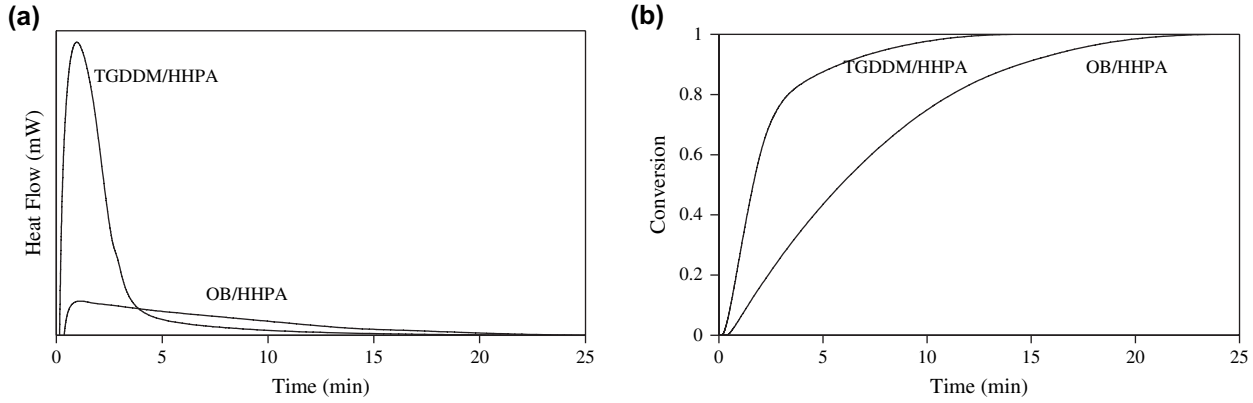

Fig. 2. (a) Isothermal DSC thermograms of TGDDM/HHPA and OB/HHPA systems at 140 °C; (b) conversion as a function of time for TGDDM/HHPA and OB/HHPA systems derived from (a).

the universal gas constant. The value of E_a can be obtained by plotting $\ln(q/T_{peak}^2)$ versus $1/T_{peak}$.

The Ozawa method yields a simple relationship between the activation energy E_a, heating rate q, and the iso-conversion temperature T, giving the activation energy as:

$$E_a = \frac{-R}{1.052}\frac{\Delta \ln q}{\Delta(1/T)} \quad (2)$$

Fig. 3 shows the DSC thermograms from the dynamic heating experiments conducted at rates between 5 and 20 °C/min. The two exotherm peaks are due to the etherification and esterification reactions as discussed earlier. By applying the Kissinger and Ozawa methods, the activation energies can be calculated from the slope of the lines presented in Fig. 4.

Table 2 summarizes the results obtained from the dynamic kinetic analysis. Linear relationships were obtained, confirming the validity of the models for the systems under study. The activation energies calculated based on the two models were in close agreement. The analysis shows that the OB/HHPA system has significantly higher activation energy than that of the TGDDM/HHPA system, entailing that the rate of the reaction between TGDDM and HHPA will increase faster with temperature than the one between OB and HHPA even with a relatively high concentration of the catalyst. From the isothermal and dynamic DSC analyses, we may derive that the reaction between TGDDM and HHPA is faster than that between OB and HHPA in the temperature range studied. Thus, it is highly likely that OB would not be incorporated well into the network if OB, TGDDM and HHPA were mixed together to react simultaneously.

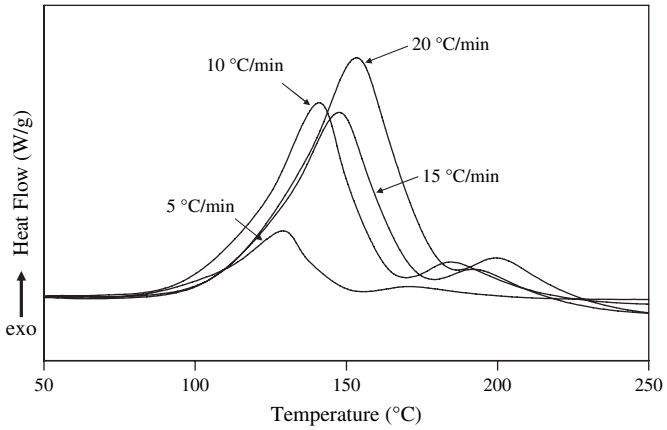

Fig. 3. Typical dynamic DSC thermograms of the OB/HHPA system.

3.3. Effect of pre-mixing

In order for OB to be well connected to the network, it was allowed to react with HHPA first *via* pre-mixing (Stage I). TGDDM was then mixed with the precursors for further curing (Stage II). To investigate the effectiveness of Stage I reaction, DSC, FTIR and SEC techniques were used to monitor the progress of the reaction as a function of time. Fig. 5 displays a typical isothermal DSC thermogram of an OB/HHPA mixture with 5 mol.% OB (epoxide/anhydride molar ratio = 5/50) under simulated pre-mixing conditions. It was observed that the maximum reaction rate was reached at about 14 min before tapering off as the time increased.

FTIR was used to follow the changes in the functional groups of the reaction mixture as the pre-mixing proceeded, as illustrated in Fig. 6. A strong symmetric Si–O–Si

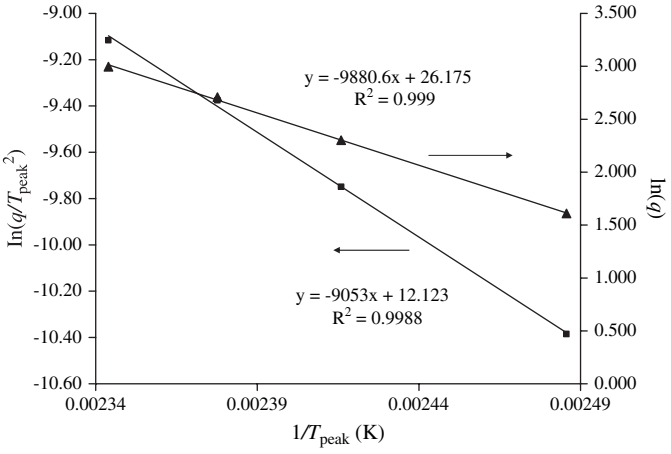

Fig. 4. Plots for the determination of activation energies of the OB/HHPA system obtained by the Kissinger and Ozawa methods.

Table 2
Peak exotherm temperatures (T) at different heating rates (q) and the corresponding activation energies (E_a) of the TGDDM/HHPA and OB/HHPA systems

q (°C/min)	T (°C)	
	TGDDM/HHPA	OB/HHPA
5	115	129
10	127	141
15	135	148
20	142	154
E_a (kJ/mol)		
Kissinger	62.6	75.3
Ozawa	65.8	78.1

stretching peak at ~1100 cm^{-1}, typical of silsesquioxane cages [33], was present in all the spectra and was used as an internal reference. It can be observed that the asymmetric stretching C=O band of HHPA at ~1898 to 1838 cm^{-1} decreased in intensity slightly while its corresponding symmetric stretching band at ~1824 to 1742 cm^{-1} sharpened as the pre-mixing reaction proceeded [34]. The anhydride C=O groups were converted to the aliphatic C=O ester bonds due to the esterification reaction between HHPA and the oxirane groups of OB. This is evident from the growing aliphatic ester stretching band at ~1745 to 1715 cm^{-1} [34]. A quantitative analysis of the conversion of the functional groups based on FTIR spectra is, however, not possible due to the overlapping of the bands.

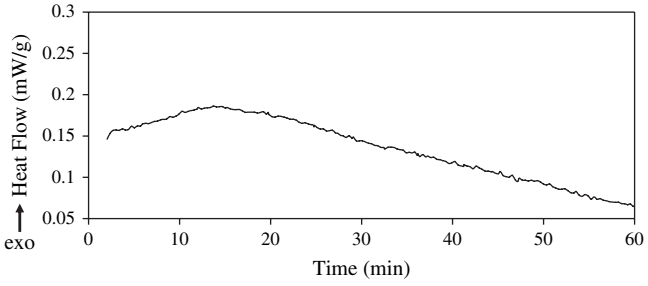

Fig. 5. Isothermal DSC thermogram of 5 mol.% OB/HHPA under the simulated pre-mixing condition, i.e. at 110 °C.

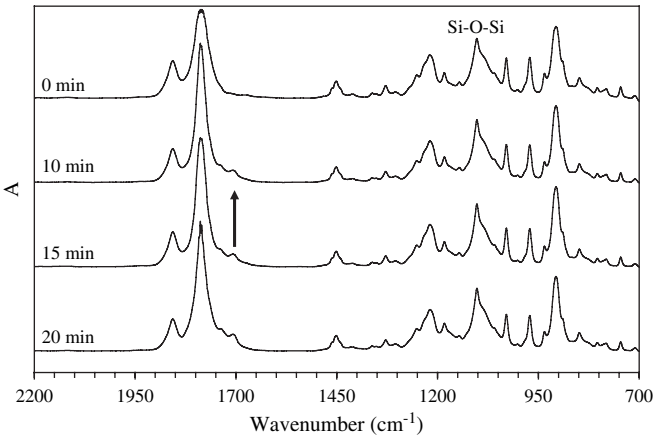

Fig. 6. Evolution of the FTIR spectrum of 5 mol.% OB/HHPA during the pre-mixing reaction.

Fig. 7 shows the SEC chromatograms of the reaction mixture at various pre-mixing time. It can be seen that as the pre-mixing time increased, HHPA content in the mixture decreased, which signifies that the reaction between OB and HHPA has taken place. At the starting point (0 min), the mass distribution curve (inset in Fig. 7) already shows a broadening on the right side of the spectrum, i.e. the higher molecular weight side, which implies that the reaction may have started before the system reached 110 °C. The increase in molecular weight at this stage is mainly due to the attachment of HHPA to OB since the fraction of the molecules with molecular weight higher than 3000, which is roughly the sum of the formula weights of one OB and eight HHPA molecules, is relatively small. A small fraction of OB dimers may have been formed, as illustrated in Scheme 3. After 10 min of pre-mixing, a tail appears on the high molecular weight side. This signifies that reaction between HHPA and oxirane groups of OB have led to the formation of a significant amount of OB dimers and trimers. When the reaction mixture was quenched to room temperature, it remained as a low-viscosity liquid. As the pre-mixing time increased to 15 min, the tail extended more to the right with the major peak becoming narrower as more OB dimers, trimers and even oligomers have formed

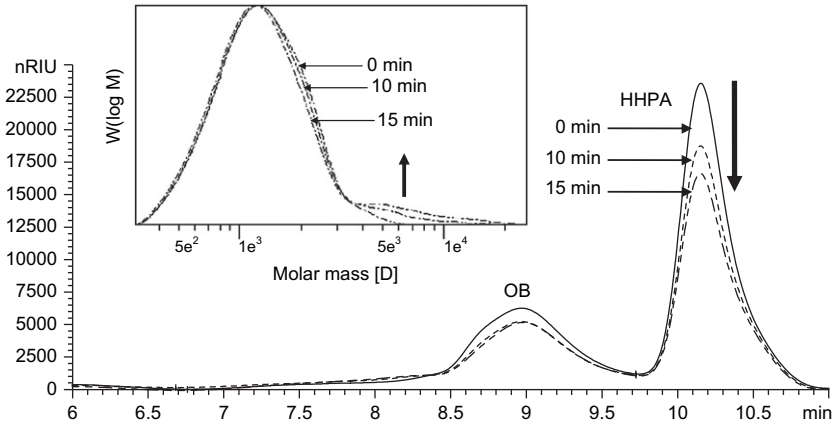

Fig. 7. Evolution of SEC chromatograms of a 5 mol.% OB/HHPA reaction mixture in Stage I; the inset is the mass distribution curves.

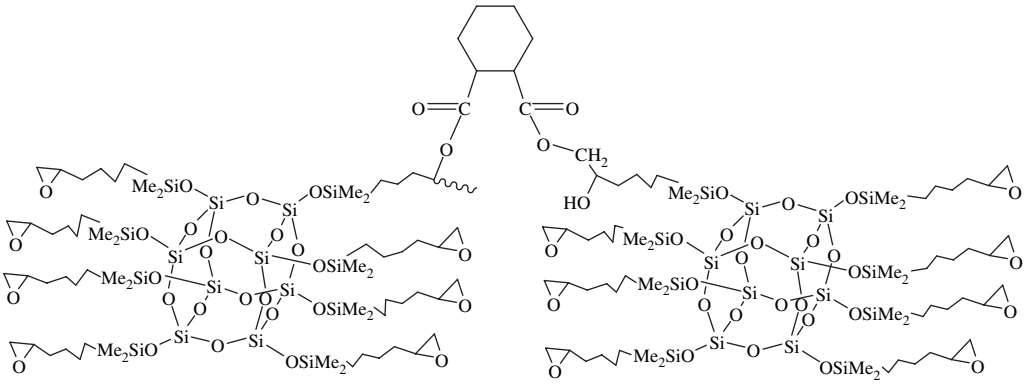

Scheme 3. Chemical structure of the "dimer", i.e. two OB molecules attached to a HHPA molecule, formed in Stage I.

although the viscosity of the reaction mixture was still fairly low at room temperature due to the excess amount of HHPA. At 20 min, the viscosity became too high for homogeneity of the system to be maintained when TGDDM was added at room temperature.

The morphology of the hybrids was examined using SEM. The micrographs are shown in Fig. 8. With no pre-mixing (A and D), some irregular-shaped white regions of ~0.3 to 1.0 μm can be observed, which are likely to be POSS-rich domains. This may be caused by the higher rate of cure between the TGDDM–HHPA reaction pair, thus OB was excluded and aggregated together to form POSS-rich domains. With the inclusion of the pre-mixing step (B and E), submicron-sized particles can be observed but their population is very small. The particles are likely to be POSS-rich clusters, i.e. OB oligomers, formed during the pre-mixing. With prolonged pre-mixing time, i.e. 20 min (C and F), the population of the POSS-rich clusters increased, which implies that more OB oligomers were formed during the pre-mixing.

Properties of the hybrids are strongly dependent on how well the POSS cages are incorporated into the networks. The dependence of the T_g of the hybrids on Stage I reaction becomes evident in Fig. 9. Without the pre-mixing, the T_g achieved was much lower than that of the hybrid prepared *via* the two-stage cure. This can be attributed to the higher reactivity of the epoxide groups on TGDDM and the increasing steric hindrance during the curing process, which resulted in the absence of anhydride molecules around OB so that a large number of epoxide groups on OB were not bonded to the network till the end of the post-cure. The cross-linking density is thus not effectively boosted by the addition of OB, and the unreacted flexible tethers may also act as 'plasticizers',

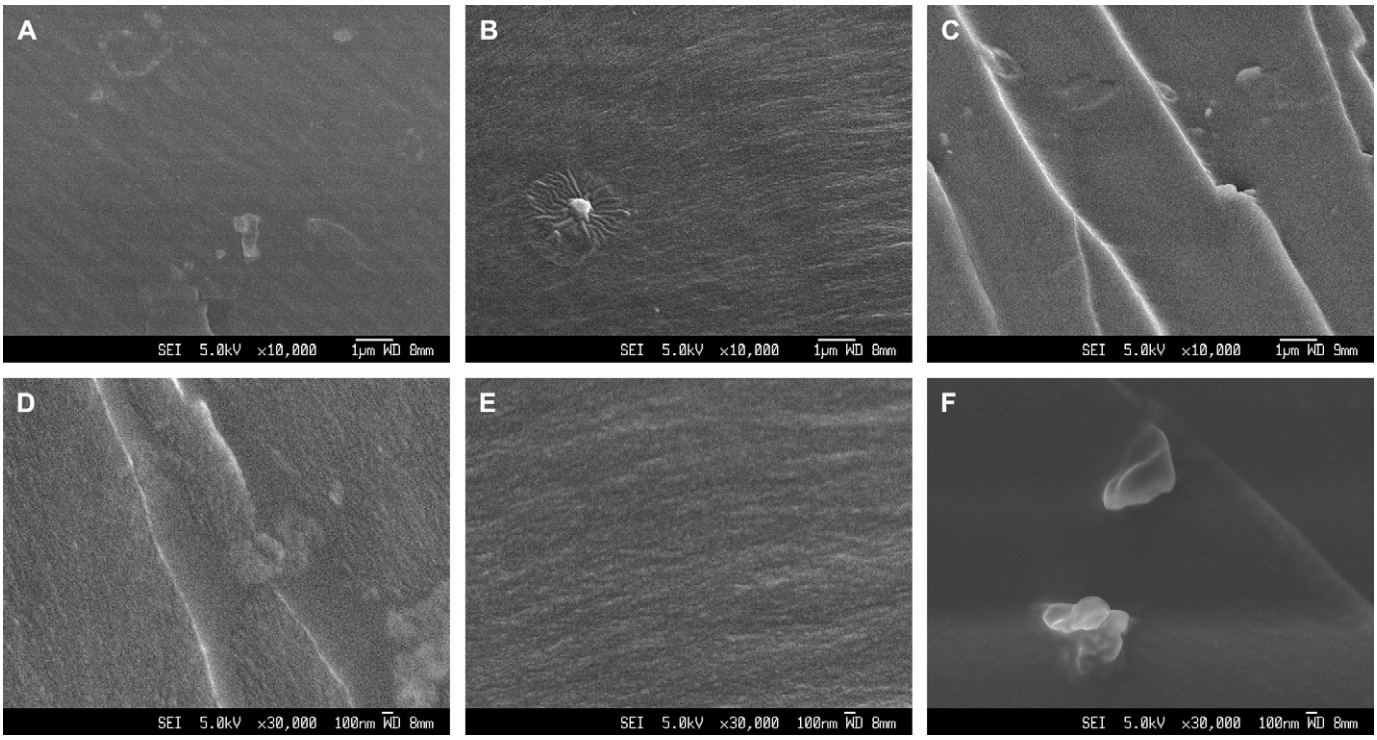

Fig. 8. SEM micrographs of the fractured surfaces of 5 mol.% OB hybrid materials with various pre-mixing times: (A and D) 0 min, (B and E) 10 min, (C and F) 20 min.

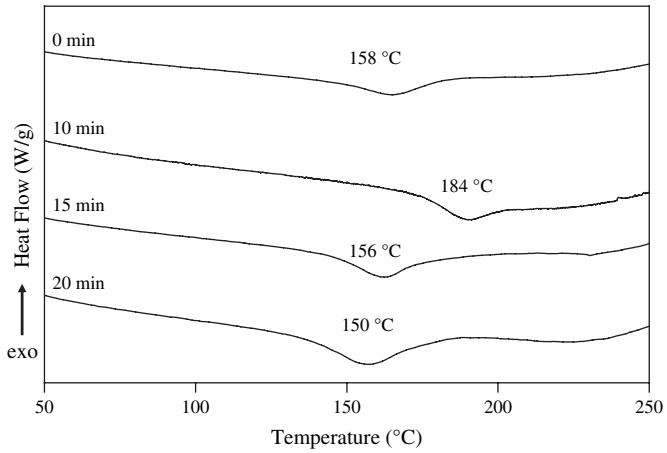

Fig. 9. DSC thermograms depicting T_gs of the hybrids containing 5 mol.% OB at different pre-mixing times. The resins were cured at 140 °C for 1 h and post-cured at 200 °C for 24 h.

permitting easier chain segmental movement. However, if the pre-mixing time was too long, the formation of OB oligomers also led to low cross-linking density, bringing about a significant reduction in T_g.

3.4. Effect of post-cure time

Due to the relatively low reactivity of OB compared to TGDDM, post-cure was necessary to improve the overall properties of the resins. To prevent the thermal oxidative degradation of the anhydride-cured resins, post-cure was carried out in argon for different time periods. It was found that T_g increased with the post-cure time, as depicted in Fig. 10, due to the increase in the cross-linking density. However, it was found that with prolonged post-cure time, i.e. 72 h, the epoxy resins yielded poorer thermo-mechanical properties. This suggested that thermal degradation of the epoxy resin might have taken place, albeit slower than in air. Hence, post-cure time was limited to 24 h for our further studies on properties.

3.5. Thermal properties

Table 3 summarizes the thermal properties of the hybrid networks. OB/HHPA shows very poor thermal properties, except its $T_d^{5\%}$, due to the presence of a large amount of flexible chains, and the molecular geometry and low reactivity of OB, which leave a large amount of flexible organic tethers unbonded to the network. The increase in the catalyst concentration by 10 times (OB/HHPA-H) improved the properties only slightly.

The $T_d^{5\%}$ improved for all OB-modified networks. The $T_d^{5\%}$ is obviously dependent on the OB concentration, suggesting that the amount of the inorganic POSS cages in the resins influences the thermal stability of the resins significantly.

A large jump of ~20 °C in T_g, as compared to TGDDM/HHPA, was observed with the addition of 5 mol.% OB, which is equivalent to 11 wt.% OB, into the resin (5 mol.% OB-10). The increase was mainly due to the high cross-linking density resulted from the bonding of the organic tethers of OB onto the network. In contrast to $T_d^{5\%}$, when the OB loading was increased to 10 mol.% (10 mol.% OB-10), T_g dropped with the same pre-mixing and cure conditions. The high functionality of OB can produce an increase in cross-linking density and hence T_g, while the flexibility of the organic arms on OB can lead to a decrease in T_g. These two counteracting effects justify the presence of a maximum T_g as a function of OB loading. In addition, the lower T_g for 10 mol.% OB-10 may also be caused by the increased probability of the formation of OB oligomers during the pre-mixing when the amount of OB molecules per unit volume was higher. With a higher catalyst concentration (5 mol.% OB-10-H), T_g was improved further due to the increase in the degree of conversion, which was, however, accompanied by a decrease in the homogeneity of the resin, as discussed below.

Dynamic mechanical analyses showed that the storage moduli (E') of the glass state of the hybrid with 5 mol.% OB increased slightly at 50 °C, as compared to TGDDM/HHPA. The increase may be attributed to the incorporation of the rigid POSS cages. However, for the hybrid with 10 mol.% OB cured

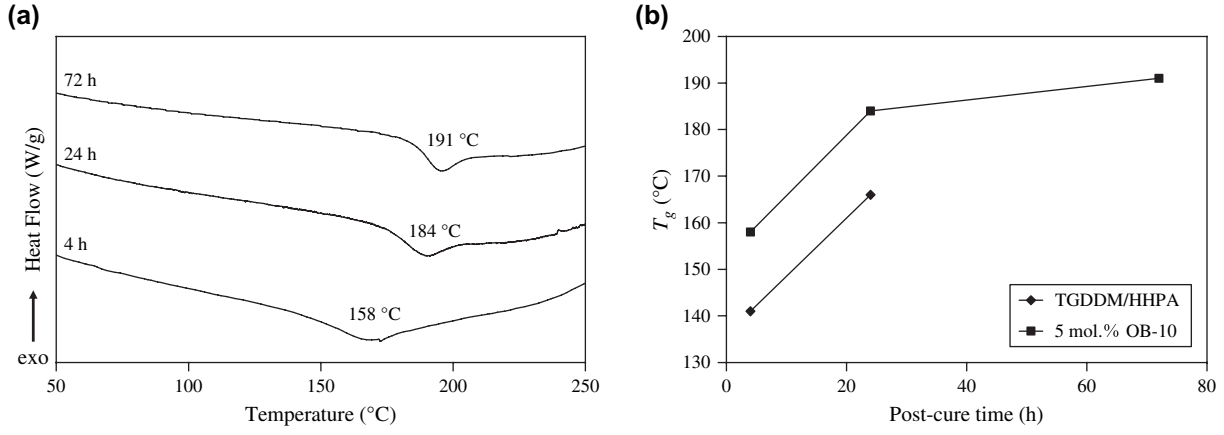

Fig. 10. (a) DSC thermograms depicting T_gs of the hybrids containing 5 mol.% OB (pre-mixing time = 10 min) at different post-cure times; (b) T_gs of the hybrids as a function of post-cure time.

Table 3
Summary of thermal and thermo-mechanical properties of the resins

Sample	T_g (°C)	$T_d^{5\%}$ (°C)	E' (MPa)			CTE (μm/m °C)	
			50 °C	100 °C	220 °C	30–50 °C	50–100 °C
TGDDM/HHPA	166	337	2536	2274	45	62	70
5 mol.% OB-10	184	344	2635	2248	61	68	78
5 mol.% OB-10-H	188	342	2268	1965	85	61	71
10 mol.% OB-10	180	354	2070	1714	94	69	87
OB/HHPA	–	379	357	140	142	146	191
OB/HHPA-H	–	378	1094	394	290	267	260

under the same conditions (10 mol.% OB-10), the glassy E' decreased by a significant amount, as compared to that of 5 mol.% OB-10. A possible explanation may be that there is inhomogeneity in the POSS distribution as OB oligomers were formed during the pre-mixing stage and the first cure. Cross-linking density was low in these areas; the organic tethers thus act as plasticizers, facilitating deformation. The increase in the catalyst concentration led to an increase in the cross-linking density as evidenced by the higher rubbery modulus of 5 mol.% OB-10-H (curve c in Fig. 11) than that of 5 mol.% OB-10 (curve b in Fig. 11). The glassy E' was, however, decreased due to the inhomogeneity of the resin caused by the very fast curing of TGDDM during the pre-mixing and the first cure at 140 °C. It can also be observed that the OB/HHPA networks (e and f) showed a significantly higher rubbery modulus than the rest of the resins due to the high cross-linking density resulting from the high POSS fractions in the resins. However, the presence of large amount of flexible organic tethers leads to much lower T_gs (below room temperature).

The TMA measurements indicate that with the addition of OB, the CTE values of the hybrids were slightly higher than that of TGDDM/HHPA. He et al. suggested that the increased CTE was due to the flexible organic tethers forming a large amount of soft interphase around the POSS cages in the resins [7]. In the present case, this can also be attributed to the incomplete cure of the organic tethers on OB.

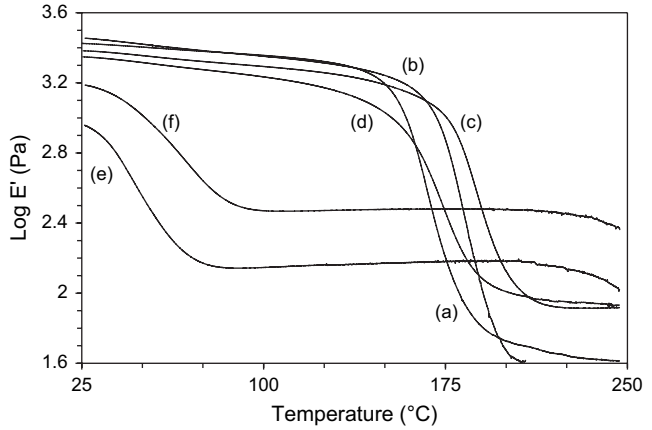

Fig. 11. Storage modulus as a function of temperature for (a) TGDDA/HHPA; (b) 5 mol.% OB-10; (c) 5 mol.% OB-10-H; (d) 10 mol.% OB-10; (e) OB/HHPA; (f) OB/HHPA-H.

4. Conclusions

A new class of epoxy-POSS/anhydride hybrid networks has been prepared using a two-stage cure method. As evidenced from the kinetics data, OB has lower reactivity than TGDDM; hence a pre-mixing reaction was necessary to enhance bonding of the OB tethers to the networks for improved properties. SEM studies have shown that pre-mixing helps to improve the homogeneity of the resins. By introducing 5 mol.% OB into the networks, the hybrid prepared *via* the optimized two-stage reactions displayed a large jump of ~20 °C in T_g, which was accompanied by slight improvements in T_d and E', while CTE was increased slightly, as compared to TGDDM/HHPA. The increased OB loading of 10 mol.% in the hybrids caused the global properties to reduce, which can be ascribed to the incomplete cure of the networks and the formation of large OB oligomers that de-homogenize the networks.

Acknowledgements

The authors thank Delphi Automotive Systems Singapore Pte. Ltd. and Nanyang Technological University, Singapore for funding of this work.

References

[1] Li GZ, Wang LC, Ni HL, Pittman Jr CU. J Inorg Organomet Polym 2001;11:123.
[2] Lee A, Lichtenhan JD. Macromolecules 1998;31:4970.
[3] Choi J, Harcup J, Yee AF, Zhu Q, Laine RM. J Am Chem Soc 2001;123:11420.
[4] Laine RM, Choi J, Lee I. Adv Mater 2001;13:800.
[5] Li G, Wang L, Toghiani H, Daulton TL, Koyama K, Pittman Jr CU. Macromolecules 2001;34:8686.
[6] Pellice SA, Fasce DP, Williams RJJ. J Polym Sci Part B Polym Phys 2003;41:1451.
[7] Huang J, Xiao Y, Mya KY, Liu X, He C, Dai J, et al. J Mater Chem 2004;14:2858.
[8] Mya KY, He C, Huang J, Xiao Y, Dai J, Siow Y-P. J Polym Sci Part A Polym Chem 2004;42:3490.
[9] Strachota A, Kroutilová I, Kovářová J, Matějka L. Macromolecules 2004;37:9457.
[10] Matějka L, Strachota A, Pleštil J, Whelan P, Steinhart M, Šlouf M. Macromolecules 2004;37:9449.
[11] Ni Y, Zheng S, Nie K. Polymer 2004;45:5557.
[12] Chen WY, Wang YZ, Kuo SW, Huang CF, Tung PH, Chang FC. Polymer 2004;45:6897.
[13] Liu H, Zheng S, Nie K. Macromolecules 2005;38:5088.
[14] Lee L-H, Chen W-C. Polymer 2005;46:2163.

[15] Liu Y, Zheng S, Nie K. Polymer 2005;46:12016.
[16] Ni Y, Zheng S. Macromol Chem Phys 2005;206:2075.
[17] Xu H, Yang B, Gao X, Li C, Guang S. J Appl Polym Sci 2006;101:3730.
[18] Choi J, Kim SG, Laine RM. Macromolecules 2004;37:99.
[19] Sulaiman S, Brick CM, Sana CMD, Katzenstein JM, Laine RM, Basheer RA. Macromolecules 2006;39:5167.
[20] Liu Y-L, Chang G-P. J Polym Sci Part A Polym Chem 2006;44:1869.
[21] Liu Y-L, Chang G-P, Hsu K-Y, Chang F-C. J Polym Sci Part A Polym Chem 2006;44:3825.
[22] Xiao F, Sun Y, Xiu Y, Wong CP. J Appl Polym Sci 2007;104:2113.
[23] Bouillon N, Pascault J-P, Tighzert L. J Appl Polym Sci 1989;38:2103.
[24] Reddy PV, Thiagarajan R, Ratra MC. J Appl Polym Sci 1990;41:319.
[25] Ellis B. Chemistry and technology of epoxy resins. London: Chapman & Hall; 1993.
[26] Fischer RF. J Polym Sci 1960;44:155.
[27] Park WH, Lee JK. J Appl Polym Sci 1998;67:1101.
[28] Rocks J, George GA, Vohwinkel F. Polym Int 2003;52:1758.
[29] Kissinger HE. Anal Chem 1957;29:1702.
[30] Flynn JH, Wall LA. J Polym Sci Part B Polym Lett 1966;4:323.
[31] Ozawa T. J Therm Anal 1970;2:301.
[32] Boey FYC, Qiang W. Polymer 2000;41:2081.
[33] Marcolli C, Calzaferrit G. Appl Organomet Chem 1999;13:213.
[34] Socrates G. Infrared characteristic group frequencies. New York: John Wiley & Sons; 1994.